Journal of *Marine Science and Engineering*

MDPI

Article

Propagation Properties of an Off-Axis Hollow Gaussian-Schell Model Vortex Beam in Anisotropic Oceanic Turbulence

Xinguang Wang [1,2], Le Wang [1] and Shengmei Zhao [1,2,3,*]

[1] Institute of Signal Processing and Transmission, Nanjing University of Posts and Telecommunications, Nanjing 210003, China; xg-cgb@njupt.edu.cn (X.W.); lewang@njupt.edu.cn (L.W.)
[2] Key Lab of Broadband Wireless Communication and Sensor Network Technology, Ministry of Education, Nanjing 210003, China
[3] State Key Laboratory of Low-Dimensional Quantum Physics, Tsinghua University, Beijing 100084, China
* Correspondence: zhaosm@njupt.edu.cn

Abstract: Based on the extended Huygens–Fresnel principle and the power spectrum of anisotropic oceanic turbulence, the analytical expressions of the average intensity and coherence properties of an off-axis hollow Gaussian-Schell model (OAHGSM) vortex beam propagating through anisotropic oceanic turbulence were derived. The effects of turbulent ocean and beam characteristic parameters on the evolution properties of the OAHGSM vortex beam were analyzed in detail. Our numerical simulation results showed that the OAHGSM vortex beam with a larger position factor is more focusable. Meanwhile, the OAHGSM vortex beam eventually evolves into a Gaussian-like beam after propagating through the anisotropic oceanic turbulent channel. The speed of this process can be accelerated by the decrease of the hollow order, topological charge, beam width, and transverse coherence width of the beam. The results also indicated that the normalized average intensity spreads more greatly and the spectral degree of coherence decays more rapidly for the smaller dissipation rate of the kinetic energy per unit mass of fluid, the smaller anisotropic coefficient, the smaller inner scale factor, the larger dissipation rate of the mean-squared temperature, and the higher temperature–salinity contribution ratio.

Keywords: vortex beam; average intensity; coherence properties; oceanic turbulence

Citation: Wang, X.; Wang, L.; Zhao, S. Propagation Properties of an Off-Axis Hollow Gaussian-Schell Model Vortex Beam in Anisotropic Oceanic Turbulence. *J. Mar. Sci. Eng.* **2021**, *9*, 1139. https://doi.org/10.3390/jmse9101139

Academic Editor: Anatoly Gusev

Received: 9 September 2021
Accepted: 13 October 2021
Published: 17 October 2021

1. Introduction

With the rise and development of underwater wireless optical communication and ocean remote sensing and imaging applications, more and more attention has been paid to the optical beams' properties, such as the degree of coherence, the degree of polarization, the effective beam widths, and the average intensity of various kinds of laser beams propagating through a turbulent ocean environment [1–11].

Owing to the extensive applications of the partially coherent beam and vortex beam carrying orbital angular momentum [12–21] in optical communication, the studies related to the typically partially coherent Gaussian-Schell model (GSM) vortex beam have aroused extensive research interests [22–27]. For instance, Wang et al. investigated the focusing properties of a GSM vortex beam [22], and Liu et al. studied the generation and propagation of an electromagnetic GSM vortex beam through a paraxial ABCD optical system [23]. The propagation of the multi-Gaussian-Schell model (MGSM) vortex beam through a stigmatic ABCD optical system [24] and isotropic random media [25] and the influence of the uniaxial crystal on partially coherent MGSM vortex beams [26] have been analyzed, respectively.

On the other hand, most beams are off-axis in the practical case, so it is of practical significance to study the propagation properties of off-axis beams [28–34]. For example, Zheng investigated the Fourier transform for a partially coherent off-axis Gaussian Schell model (OAGSM) beam [28]. Cai et al. worked on the propagation of an OAGSM beam

through atmospheric turbulence [29]. The propagation properties of an off-axis hollow vortex Gaussian beam [30–32] in free space, off-axis MGSM hollow vortex beams in free space, and isotropic oceanic turbulence [33] have also been investigated in detail.

Recently, Song et al. studied the propagation of an autofocusing OAHGSM vortex beam through atmospheric turbulence [34]. Compared with atmospheric turbulence, the mechanism of the influence of oceanic turbulence on beam propagation is fundamentally different. In the study of the turbulence effect of optical wave propagation, the impact of the refractive index fluctuation of turbulent media is the key point, which for atmospheric turbulence mainly depends on the temperature change, while that for oceanic turbulence arises from the variation of temperature and salinity [35]. Meanwhile, there exists a low loss window at the blue-green band of oceanic turbulence [36], which is distinct from that at the optical waves of atmospheric turbulence. Additionally, oceanic turbulence will be anisotropic due to the Earth's rotation [21]; the strength of atmospheric turbulence can be described by the refractive index structure constant [37], while that of anisotropic oceanic turbulence is more complicated, which is characterized by the comprehensive effect of various oceanic turbulence parameters [27].

Due to the significant difference between atmospheric and oceanic turbulence on the propagation of optical waves, together with the increasing demand for underwater wireless optical communication, it is very interesting to investigate the propagation of an OAHGSM vortex beam in the turbulent ocean environment. However, to the best of our knowledge, the propagation properties of an OAHGSM vortex beam passing through anisotropic oceanic turbulence have not been explored. In this paper, we study the average intensity and coherence properties of an OAHGSM vortex beam in anisotropic oceanic turbulence, investigate how the beam parameters affect these properties, and analyze the dependence of the anisotropic oceanic turbulence effect on turbulent medium parameters to explore how anisotropic oceanic turbulence affects the propagation of an OAHGSM vortex beam in it.

The contribution of this paper is that we investigated the propagation properties of the OAHGSM vortex beam in anisotropic oceanic turbulence, where anisotropic oceanic turbulence is closer to the actual seawater environment than isotropic oceanic turbulence. Hence, the work enriches the research work on underwater communication channel modeling, and the results are helpful for the design and application of underwater wireless optical communication. In addition, the results in the paper show that the OAHGSM vortex beam is more affected by anisotropic oceanic turbulence when the beam parameters (N, M, σ, ω_0) are smaller, the turbulence parameters ε, ζ, η are smaller, and the turbulence parameters χ_t, ϖ are bigger, which provides the parameter setup strategy for the OAHGSM vortex beam in underwater wireless optical communication systems.

The organization of this paper is as follows. Firstly, we derive the analytical formula of the strength of anisotropic oceanic turbulence, analyze the influence of various parameters on the turbulence effect, and derive the analytical formulas for the average intensity, as well as the spectral degree of coherence of the OAHGSM vortex beam. Secondly, we numerically explore the effect of different beam and turbulent ocean characteristic parameters on the average intensity and the spectral degree of coherence of the OAHGSM vortex beam in detail. Then, we discuss the results. Finally, we summarize the paper.

2. Theoretical Analysis

In the Cartesian coordinate system, the amplitude of an off-axis hollow beam at the source plane $z = 0$ takes the form [33,34]:

$$E(\rho_0, 0) = \Omega_0[(x_0 - A_x)^2 + (y_0 - A_y)^2]^N[(x_0 - A_x) + i(y_0 - A_y)]^M \exp(-\frac{x_0^2 + y_0^2}{\omega_0^2}) \quad (1)$$

where x_0, y_0 are the Cartesian components of the arbitrary position vector ρ_0, which is located at the plane z; Ω_0 is a constant; ω_0 is related to the width of the Gaussian beam;

(A_x, A_y) is the position of the hollow and vortex factor; N and M denote the hollow order and topological charge, respectively.

Based on the unified theory of coherence and polarization [38], the cross-spectral density (CSD) function of an OAHGSM vortex beam, generated by anisotropic Gaussian-Schell model sources, emerging from two spatial positions ρ_{10} and ρ_{20} in the source plane, can be written as [34,39]:

$$\begin{aligned} W(\rho_{10},\rho_{20},0) &= \Omega_0[(x_{10}-A_x)^2+(y_{10}-A_y)^2]^N[(x_{10}-A_x)+i(y_{10}-A_y)]^M \exp(-\frac{x_{10}^2+y_{10}^2}{\omega_0^2}) \\ &\times \Omega_0[(x_{20}-A_x)^2+(y_{20}-A_y)^2]^N[(x_{20}-A_x)-i(y_{20}-A_y)]^M \exp(-\frac{x_{20}^2+y_{20}^2}{\omega_0^2}) \\ &\times \exp[-\frac{(x_{10}-x_{20})^2}{2\sigma^2}] \exp[-\frac{(y_{10}-y_{20})^2}{2\sigma^2}] \end{aligned} \tag{2}$$

where σ characterizes the transverse coherence width.

When the beam propagates through ocean water, the cumulative effect of the refractive index fluctuation of anisotropic oceanic turbulence can be regarded as a pure complex phase perturbation on the vortex beam [13,40]. With the extended Huygens–Fresnel principle, the CSD function of an OAHGSM vortex beam at any point in the half space $z > 0$ of the turbulent ocean channel under the paraxial approximation can be derived as [5,7,11,34]:

$$\begin{aligned} W(\rho_1,\rho_2,z) &= \frac{k^2}{4\pi^2 z^2}\int_{-\infty}^{+\infty}\int_{-\infty}^{+\infty}\int_{-\infty}^{+\infty}\int_{-\infty}^{+\infty} W(\rho_{10},\rho_{20},0)\exp[-\frac{ik}{2z}(\rho_1-\rho_{10})^2+\frac{ik}{2z}(\rho_2-\rho_{20})^2] \\ &\times <\exp[\Psi(\rho_{10},\rho_1)+\Psi^*(\rho_{20},\rho_2)]> d\rho_{10}d\rho_{20} \\ &= \frac{k^2}{4\pi^2 z^2}\int_{-\infty}^{+\infty}\int_{-\infty}^{+\infty}\int_{-\infty}^{+\infty}\int_{-\infty}^{+\infty} W(\rho_{10},\rho_{20},0)\exp[-\frac{ik}{2z}(\rho_1-\rho_{10})^2+\frac{ik}{2z}(\rho_2-\rho_{20})^2] \\ &\times \exp\left\{-\frac{\pi^2k^2z}{3}\int_0^{\infty}\kappa^3\Phi_n(\kappa)d\kappa[(\rho_{10}-\rho_{20})^2+(\rho_{10}-\rho_{20})(\rho_1-\rho_2)+(\rho_1-\rho_2)^2]\right\}d\rho_{10}d\rho_{20} \\ &= \frac{k^2}{4\pi^2 z^2}\int_{-\infty}^{+\infty}\int_{-\infty}^{+\infty}\int_{-\infty}^{+\infty}\int_{-\infty}^{+\infty} W(\rho_{10},\rho_{20},0)\exp[-\frac{ik}{2z}(\rho_1-\rho_{10})^2+\frac{ik}{2z}(\rho_2-\rho_{20})^2] \\ &\times \exp[-\frac{(\rho_{10}-\rho_{20})^2+(\rho_{10}-\rho_{20})(\rho_1-\rho_2)+(\rho_1-\rho_2)^2}{\Lambda^2}]d\rho_{10}\rho_{20} \end{aligned} \tag{3}$$

where $k = 2\pi/\lambda$ denotes the wave number and λ is the wavelength. Ψ is the complex phase perturbation of a spherical wave propagating through anisotropic oceanic turbulence, and $*$ denotes the complex conjugate. $<\cdot>$ denotes averaging over the ensemble of anisotropic turbulent ocean, and:

$$\Lambda = [k^2 z \Lambda_0]^{-1/2} \tag{4}$$

$$\Lambda_0 = \pi^2/3\int_0^{\infty}\kappa^3\Phi_n(\kappa)d\kappa \tag{5}$$

Λ refers to the spatial coherent radius of the spherical wave propagating in a turbulent ocean; Λ_0 denotes the strength of the oceanic turbulence [27]; $\Phi_n(\kappa)$ is the spatial power spectrum of the refractive index of anisotropic ocean turbulence, which can be expressed as [21]:

$$\Phi_n(\kappa) = 0.388\times10^{-8}\chi_t\zeta^2\varepsilon^{-1/3}\kappa^{-11/3}[1+2.35(\kappa\eta)^{2/3}]\times\phi(\kappa,\varpi) \tag{6}$$

where $\phi(\kappa,\varpi) = exp(-A_T\theta)+\varpi^{-2}exp(-A_S\theta)-2\varpi^{-1}exp(-A_{TS}\theta)$, $A_T = 1.863\times10^{-2}$, $A_S = 1.9\times10^{-4}$, $A_{TS} = 9.41\times10^{-3}$, $\theta = 8.284(\kappa\eta)^{4/3}+12.978(\kappa\eta)^2$. ε is the dissipation rate of the kinetic energy per unit mass of fluid ranging from 10^{-10} m^2/s^{-3} to 10^{-1} m^2/s^{-3}. χ_t is the dissipation rate of the mean-squared temperature in the range of 10^{-10} K^2/s to 10^{-4} K^2/s. ϖ is the temperature–salinity contribution ratio varying from -5 to 0, where -5 and 0 correspond to dominating temperature-driven and salinity-driven turbulence. ζ is the anisotropic coefficient of anisotropic oceanic turbulence, and $\Phi_n(\kappa)$ reduces to the spatial power spectrum of the refractive index of isotropic ocean turbulence for $\zeta = 1$. η is

the inner scale factor of a turbulent ocean, taking values in the range from 6×10^{-5} m to 10^{-2} m.

Combining Equation (6) with Equation (5), the analytical expression of Λ_0 can be derived as:

$$\Lambda_0 = 8.705 \times 10^{-8} (\varepsilon\eta)^{-1/3} \zeta^{-2} \chi_t (1 - 2.605\varpi^{-1} + 7.007\varpi^{-2}) \quad (7)$$

When the optical beam propagates in seawater, the influence of the turbulence effect on the evolution behavior is closely related to the strength of the turbulence, which is controlled by various turbulence parameters. Based on Equation (7), we illustrate the strength of anisotropic oceanic turbulence Λ_0 versus the anisotropic coefficient ζ for different dissipation rates of the kinetic energy per unit mass of fluid ε, dissipation rates of the mean-squared temperature χ_t, the inner scale factor η, and the temperature–salinity contribution ratio ϖ in Figure 1. As shown in Figure 1, Λ_0 decreases with the increase of ε, η, and ζ and the decrease of χ_t and ϖ, which provides theoretical support for the study of the specific influence of various turbulent ocean parameters on the propagation of the OAHGSM vortex beam in seawater below.

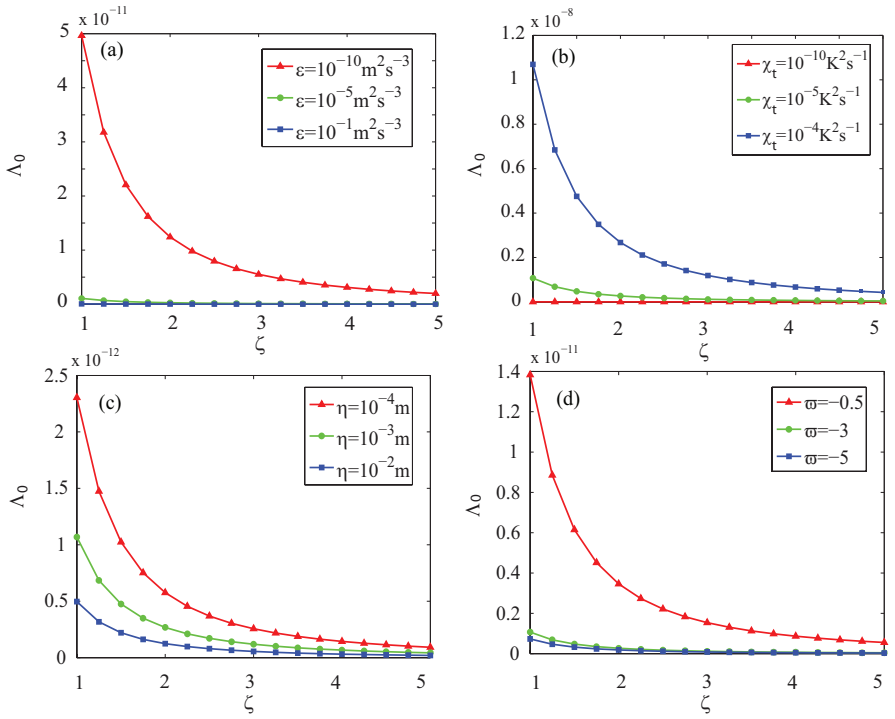

Figure 1. The strength of the anisotropic oceanic turbulence Λ_0 versus the anisotropic coefficient ζ for different dissipation rates of the kinetic energy per unit mass of fluid ε (**a**), dissipation rates of the mean-squared temperature χ_t (**b**), the inner scale factor η (**c**), and the temperature–salinity contribution ratio ϖ (**d**).

Combining Equation (7) with Equations (2)–(4) and following a similar process as in [34], we can derive the CSD function of the OAHGSM vortex beam passing through anisotropic oceanic turbulence as:

$$
\begin{aligned}
W(\rho_1,\rho_2,z) = {} & \frac{k^2}{4\pi^2 z^2}\exp[-\frac{ik}{2z}(x_1^2+y_1^2)+\frac{ik}{2z}(x_2^2+y_2^2)]\exp[-\frac{(x_1-x_2)^2+(y_1-y_2)^2}{\Lambda^2}] \\
& \times \Omega_0 \exp(-\frac{A_x^2}{\omega_0^2}-\frac{A_y^2}{\omega_0^2})\sum_{n_1=0}^{N}\frac{N!}{n_1!(N-n_1)!}\sum_{m_1=0}^{M}\frac{M!i^{m_1}}{m_1!(M-m_1)!} \\
& \times \Omega_0 \exp(-\frac{A_x^2}{\omega_0^2}-\frac{A_y^2}{\omega_0^2})\sum_{n_2=0}^{N}\frac{N!}{n_2!(N-n_2)!}\sum_{m_2=0}^{M}\frac{M!(-i)^{m_2}}{m_2!(M-m_2)!} \\
& \times \exp[-\frac{ik}{2z}[(2x_2A_x-2x_1A_x)+(2y_2A_y-2y_1A_y)]]w(x,z)w(y,z)
\end{aligned} \tag{8}
$$

where:

$$
\begin{aligned}
W(x,z) = {} & \sqrt{\frac{\pi}{e}}(2(N-n_1)+M-m_1)!\exp[\frac{1}{e}[\frac{ik}{2z}(x_1-A_x)-\frac{A_x}{\omega_0^2}-\frac{x_1-x_2}{2\Lambda^2}]^2] \\
& \times (\frac{1}{e})^{2(N-n_1)+M-m_1}\sum_{u=0}^{\frac{2(N-n_1)+M-m_1}{2}}\frac{1}{u!(2(N-n_1)+M-m_1-2u)!} \\
& \times (\frac{e}{4})^{u}\sum_{v=0}^{2(N-n_1)+M-m_1-2u}\frac{[2(N-n_1)+M-m_1-2u]!}{v!(2(N-n_1)+M-m_1-2u-v)!} \\
& \times [\frac{ik}{2z}(x_1-A_x)-\frac{A_x}{\omega_0^2}-\frac{x_1-x_2}{2\Lambda^2}]^{2(N-n_1)+M-m_1-2u-v}(\frac{1}{2\sigma^2}+\frac{1}{\Lambda^2})^{v} \\
& \times \sqrt{\frac{\pi}{f}}2^{-(2(N-n_2)+M-m_2+v)}i^{2(N-n_2)+M-m_2+v}\exp(\frac{j_x^2}{f}) \\
& \times (\frac{1}{f})^{0.5(2(N-n_2)+M-m_2+v)}H_{2(N-n_2)+M-m_2+v}(-\frac{ij_x}{\sqrt{f}})
\end{aligned} \tag{9}
$$

$$
\begin{aligned}
W(y,z) = {} & \sqrt{\frac{\pi}{e}}(2n_1+m_1)!\exp[\frac{1}{e}[\frac{ik}{2z}(y_1-A_y)-\frac{A_y}{\omega_0^2}-\frac{y_1-y_2}{2\Lambda^2}]^2] \\
& \times (\frac{1}{e})^{2n_1+m_1}\sum_{u=0}^{\frac{2n_1+m_1}{2}}\frac{1}{u!(2n_1+m_1-2u)!}(\frac{e}{4})^{u} \\
& \times \sum_{v=0}^{2n_1+m_1-2u}\frac{[2n_1+m_1-2u]!}{v!(2n_1+m_1-2u-v)!} \\
& \times [\frac{ik}{2z}(y_1-A_y)-\frac{A_y}{\omega_0^2}-\frac{y_1-y_2}{2\Lambda^2}]^{2n_1+m_1-2u-v}(\frac{1}{2\sigma^2}+\frac{1}{\Lambda^2})^{v} \\
& \times \sqrt{\frac{\pi}{f}}2^{-(2n_2+m_2+v)}i^{2n_2+m_2+v}\exp(\frac{j_y^2}{f}) \\
& \times (\frac{1}{f})^{0.5(2n_2+m_2+v)}H_{2n_2+m_2+v}(-\frac{ij_y}{\sqrt{f}})
\end{aligned} \tag{10}
$$

with:

$$
e = \frac{1}{\omega_0^2}+\frac{1}{2\sigma^2}+\frac{1}{\Lambda^2}+\frac{ik}{2z} \tag{11}
$$

$$
f = \frac{1}{\omega_0^2}+\frac{1}{2\sigma^2}+\frac{1}{\Lambda^2}-\frac{ik}{2z}-\frac{1}{e}(\frac{1}{2\sigma^2}+\frac{1}{\Lambda^2})^2 \tag{12}
$$

$$
j_x = \frac{ik}{2z}(A_x-x_2)-\frac{A_x}{\omega_0^2}+\frac{x_1-x_2}{2\Lambda^2}+\frac{1}{e}[\frac{ik}{2z}(x_1-A_x)-\frac{A_x}{\omega_0^2}-\frac{x_1-x_2}{2\Lambda^2}](\frac{1}{2\sigma^2}+\frac{1}{\Lambda^2}) \tag{13}
$$

$$j_y = \frac{ik}{2z}(A_y - y_2) - \frac{A_y}{\omega_0^2} + \frac{y_1 - y_2}{2\Lambda^2} + \frac{1}{e}[\frac{ik}{2z}(y_1 - A_y) - \frac{A_y}{\omega_0^2} - \frac{y_1 - y_2}{2\Lambda^2}](\frac{1}{2\sigma^2} + \frac{1}{\Lambda^2}) \quad (14)$$

By setting $\rho_1 = \rho_2 = \rho$, we can obtain the average intensity of the OAHGSM vortex beam passing through anisotropic oceanic turbulence at the observation plan z as [11]:

$$I(\rho, z) = W(\rho, \rho, z) \quad (15)$$

The spectral degree of coherence of two different points $\rho_1 = (x_1, y_1)$ and $\rho_2 = (x_2, y_2)$ for the OAHGSM vortex beam passing through anisotropic oceanic turbulence in the observation plane z is commonly introduced as [1,6]:

$$\mu(\rho_1, \rho_2, z) = \frac{W(\rho_1, \rho_2, z)}{[W(\rho_1, \rho_1, z)W(\rho_2, \rho_2, z)]^{\frac{1}{2}}} \quad (16)$$

3. Numerical Simulations

In this section, we investigate the average intensity and coherence properties of the OAHGSM vortex beam passing through anisotropic oceanic turbulence by numerical examples using the analytical formulas in the above section. The common numerical calculation parameters were chosen as $N = 2, M = 1, \omega_0 = 10^{-2}$ m, $\sigma = 2 \times 10^{-2}$ m, $A_x = 10^{-3}$ m, $A_y = 0, \lambda = 532 \times 10^{-9}$ m, $\varepsilon = 10^{-5}$ m^{2}s^{-3}, $\chi_t = 10^{-8}$ K^{2}s^{-1}, $\varpi = -3$, $\zeta = 2, \eta = 10^{-3}$ m, unless the specific parameters are listed in the figures.

Figure 2 shows the normalized average intensity I/I_{max} and corresponding contour graphs of the OAHGSM vortex beam propagating through anisotropic oceanic turbulence at different transmission distances. As can be seen from Figure 2a,b, the dark hollow center of the OAHGSM vortex beam can be maintained for a short transmission distance. With the increment of the transmission distance, the dark hollow center gradually disappears and the intensity distribution gradually spreads. In the far field, as shown in Figure 2d, the OAHGSM vortex beam evolves into a Gaussian-like beam.

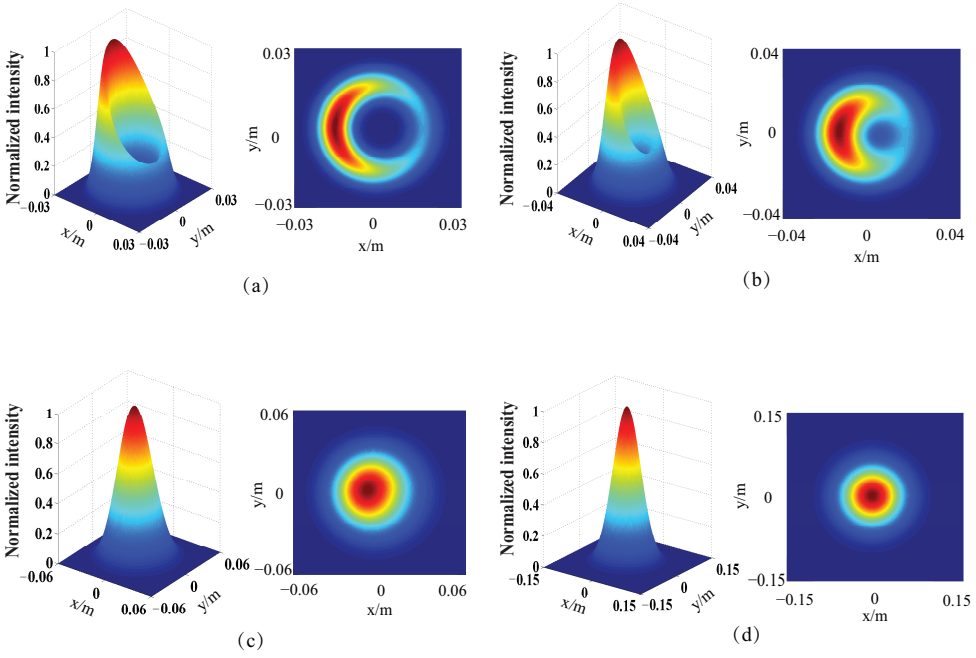

Figure 2. Normalized average intensity and corresponding contour graphs of the OAHGSM vortex beam propagating through anisotropic oceanic turbulence. (**a**) $z = 100$ m, (**b**) $z = 300$ m, (**c**) $z = 600$ m, (**d**) $z = 1200$ m.

The contour graphs of the normalized average intensity of the OAHGSM vortex beam with different position factors propagating through anisotropic oceanic turbulence

at $z = 100$ m are illustrated in Figure 3. When $A_x = A_y = 0$, the normalized intensity distribution of the OAHGSM vortex beam has a circular symmetry characteristic (Figure 3a), and this circular symmetry structure is broken for nonzero position factors. Comparing Figure 3d with Figure 3c, we can find that the focusing distribution becomes more obvious by increasing the position factor.

In order to investigate the influence of beam characteristic parameters on the average intensity, the cross lines ($y = 0$) of the normalized average intensity of the OAHGSM vortex beam passing through anisotropic oceanic turbulence with different hollow order N, topological charge M, coherence width σ, and beam width ω_0 are analyzed in Figures 4 and 5. It is observed from Figure 4 that the OAHGSM vortex beam propagating under the turbulent ocean environment can almost keep the initial dark hollow profile at a shorter propagation distance, and the hollow area is enlarged by a larger hollow order N. As the transmission distance increases, the OAHGSM vortex beam gradually loses the initial beam profile and evolves into a Gaussian-like beam in the far field. As can be seen from Figure 5, the normalized average intensity of the OAHGSM vortex beam with different M, σ and ω_0 undergoes a similar evolution process analogous to the behavior of the beam with different N.

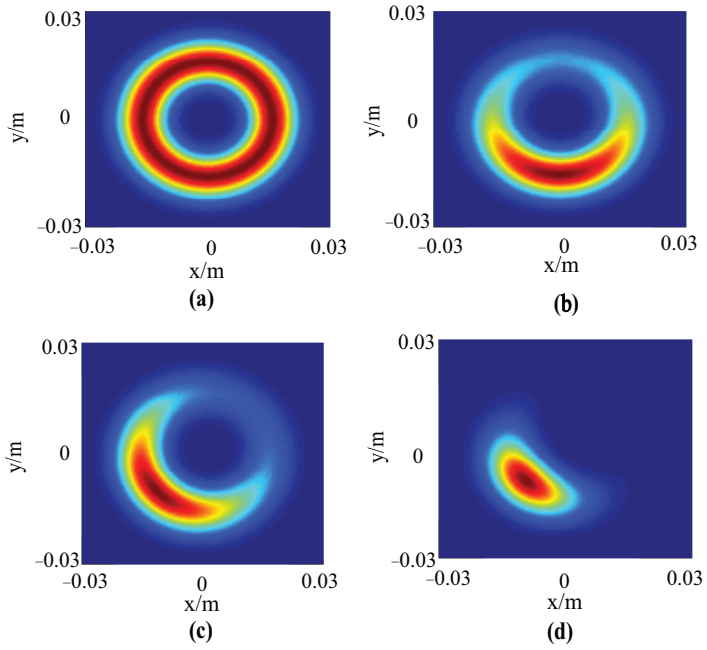

Figure 3. Contour graphs of the normalized average intensity of the OAHGSM vortex beam with different position factors propagating through anisotropic oceanic turbulence at $z = 100$ m. (**a**) $A_x = A_y = 0$, (**b**) $A_x = 0$, $A_y = 0.001$ m, (**c**) $A_x = 0.001$ m, $A_y = 0.001$ m, (**d**) $A_x = 0.005$ m, $A_y = 0.005$ m.

The influence of turbulent ocean characteristic parameters on the average intensity of the OAHGSM vortex beam passing through anisotropic oceanic turbulence and the cross lines ($y = 0$) of the normalized average intensity of the OAHGSM vortex beam with different dissipation rates of the kinetic energy per unit mass of fluid ε, dissipation rates of the mean-squared temperature χ_t, the inner scale factor η, the temperature–salinity contribution ratio ϖ, and the anisotropic coefficient ζ are shown in Figures 6 and 7. It is shown that the OAHGSM vortex beam propagating in a turbulent ocean with smaller ε, η, and ζ and larger χ_t and ϖ loses the initial dark hollow profile faster, and the beam gradually evolves into a Gaussian-like beam with the increase of the transmission distance.

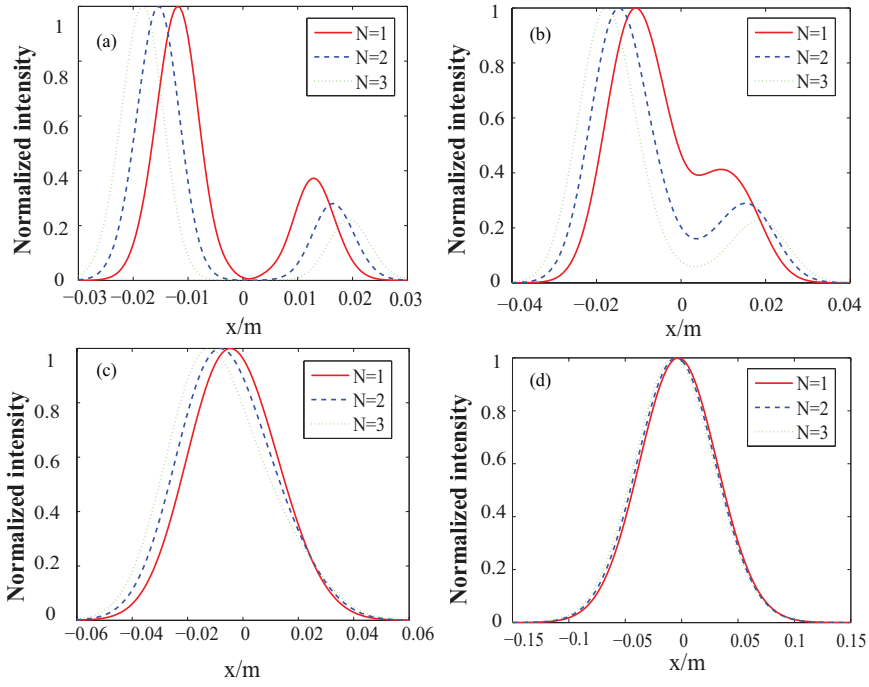

Figure 4. Cross lines ($y = 0$) of the normalized average intensity of the OAHGSM vortex beam passing through anisotropic oceanic turbulence with different hollow order N at $z = 100$ m (**a**), $z = 300$ m (**b**), $z = 600$ m (**c**), and $z = 1200$ m (**d**).

The spectral degree of coherence of the OAHGSM vortex beam between two points $\rho_1 = (x, 0)$ and $\rho_2 = (0, 0)$ passing through anisotropic oceanic turbulence with different beam characteristic parameters is shown in Figure 8. It is found from Figure 8a that the spectral degree of coherence of the OAHGSM vortex beam with different topological charges M propagating at a shorter transmission distance possesses a turning point. At the far field shown in Figure 8b, the spectral degree of the coherence curves of the OAHGSM vortex beam decreases smoothly with the increase of the transverse distance x, and the effect of the different values of M on the spectral coherence curves gradually disappears with the further increase of the transverse distance. As is shown in Figure 8c,d, the evolution behavior of the spectral degree of coherence as a function of the transverse distance x in the far field with different N and σ for OAHGSM vortex beam goes through the similar processes as in Figure 8b, and the attenuation of the spectral degree of coherence becomes faster with a larger value of N and a smaller value of σ.

Figure 9 illustrates the effect of different turbulent ocean characteristic parameters on the evolution behavior of the spectral degree of coherence of the OAHGSM vortex beam at $z = 1200$ m. It can be clearly seen from Figure 9a,b that, with the decrease of ε and the increase of ϖ, the strength of oceanic turbulence in Figure 1 increases, and the spectral degree of coherence of the OAHGSM vortex beam decreases. By comparing the two figures above, for given ε and ϖ, the spectral degree of coherence of the OAHGSM vortex beam shares a negative relationship with the transverse distance between two points, which is 0.1 cm in Figure 9a and 0.5 cm in Figure 9b. For given χ_t, η, and ζ, similar results can also be found by comparing Figure 9c–f. Furthermore, the smaller χ_t is and the larger η and ζ are, the smaller the strength of oceanic turbulence, as shown in Figure 1, is, and the greater the spectral degree of coherence of the OAHGSM vortex beam is.

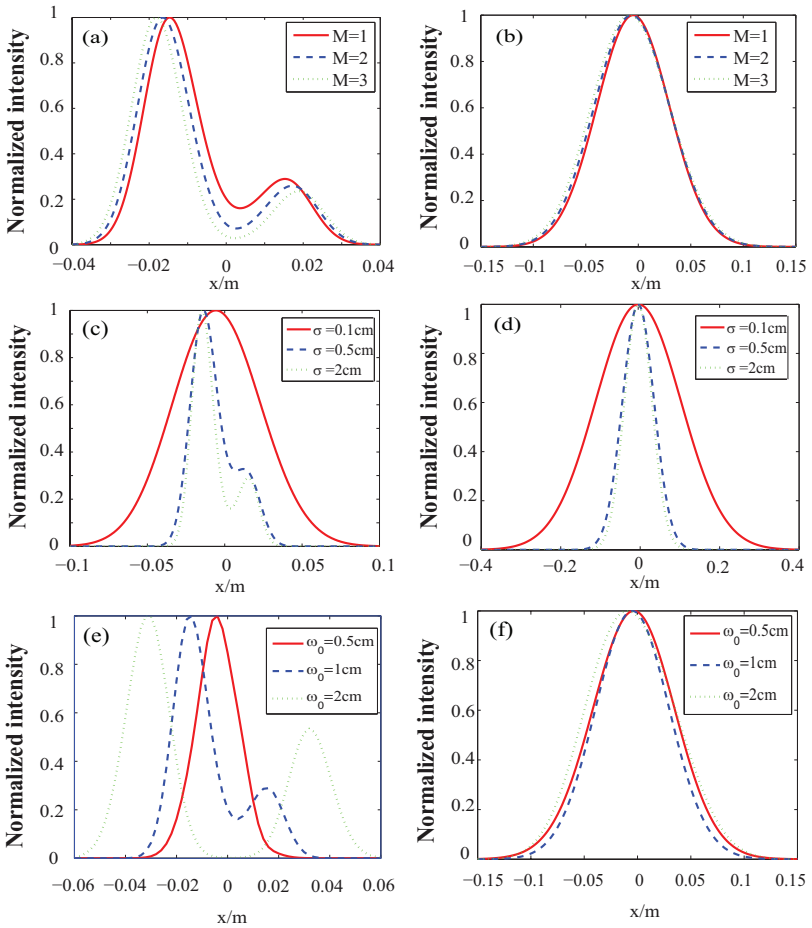

Figure 5. Cross lines ($y = 0$) of the normalized average intensity of the OAHGSM vortex beam passing through anisotropic oceanic turbulence with different M, σ, and ω_0 at $z = 300$ m (**a**), $z = 1200$ m (**b**), $z = 300$ m (**c**), $z = 1200$ m (**d**), $z = 300$ m (**e**), and $z = 1200$ m (**f**).

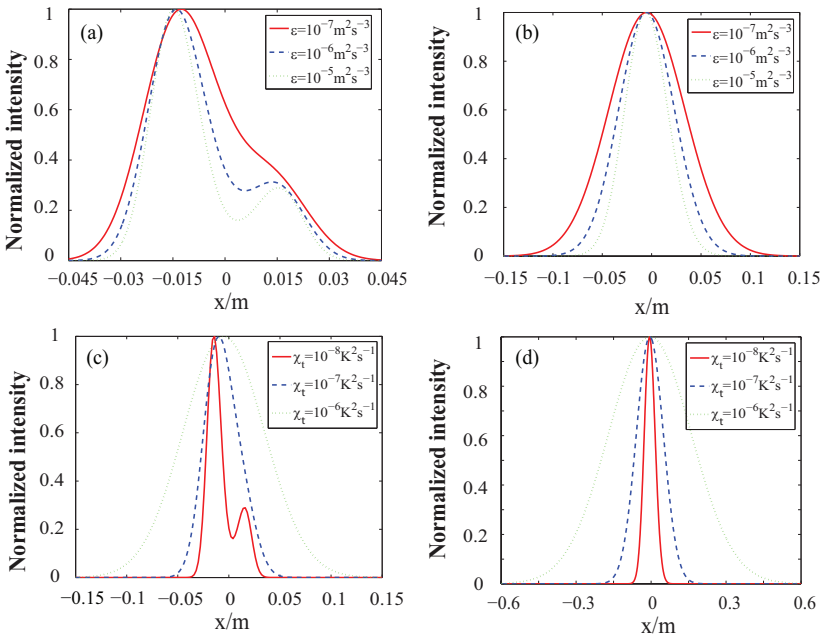

Figure 6. Cross lines (y = 0) of the normalized average intensity of the OAHGSM vortex beam passing through anisotropic oceanic turbulence with different ε and χ_t at z = 300 m (**a**), z = 800 m (**b**), z = 300 m (**c**), and z = 800 m (**d**).

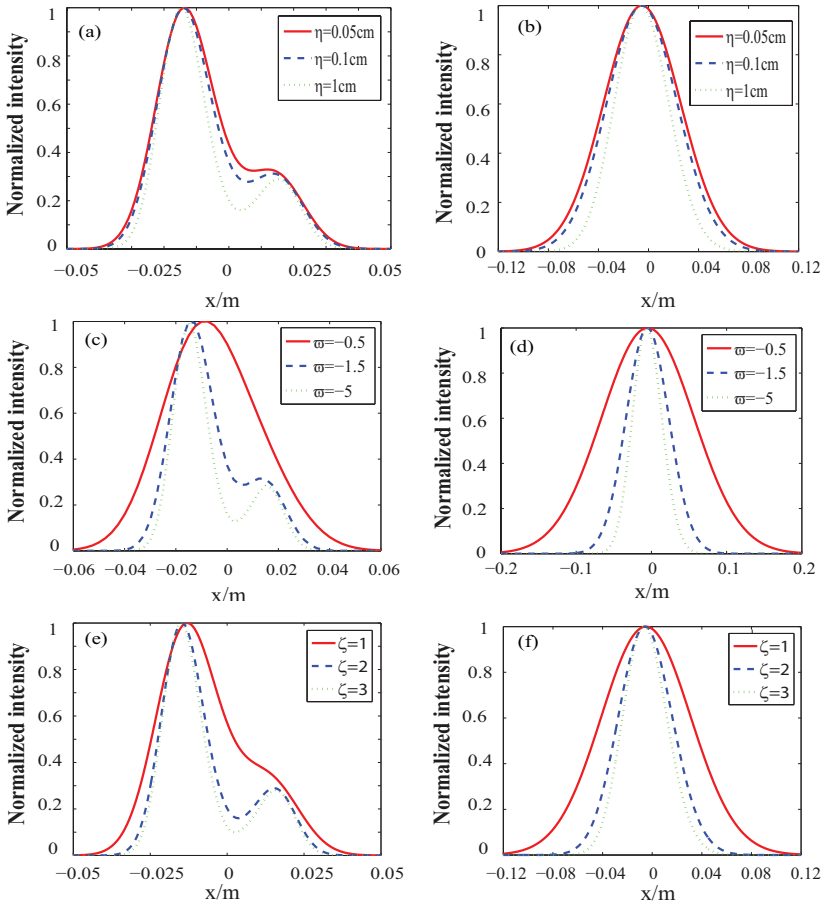

Figure 7. Cross lines ($y = 0$) of the normalized average intensity of the OAHGSM vortex beam passing through anisotropic oceanic turbulence with different η, ϖ, and ζ at z = 300 m (**a**), z = 800 m (**b**), z = 300 m (**c**), z = 800 m (**d**), z = 300 m (**e**), and z = 800 m (**f**).

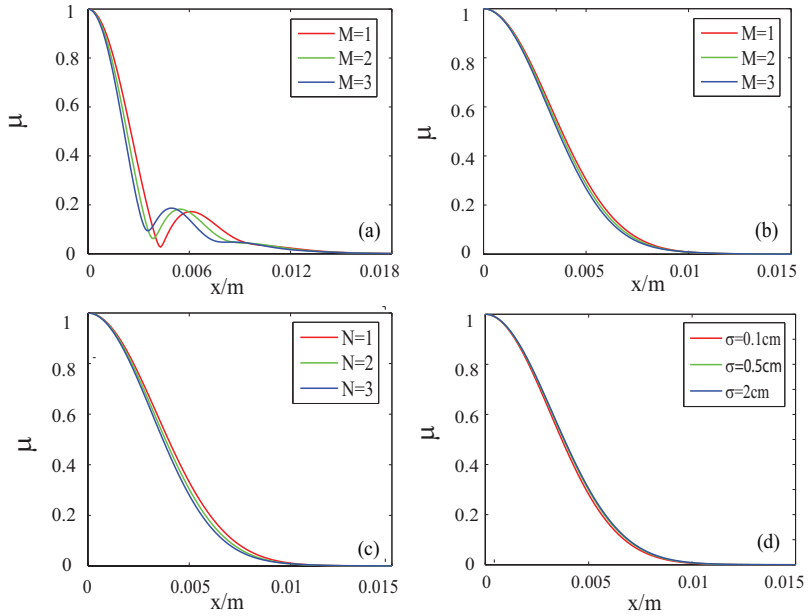

Figure 8. Spectral degree of coherence of the OAHGSM vortex beam passing through anisotropic oceanic turbulence with different M, N, and δ at $z = 300$ m (**a**), $z = 1200$ m (**b**), $z = 1200$ m (**c**), and $z = 1200$ m (**d**).

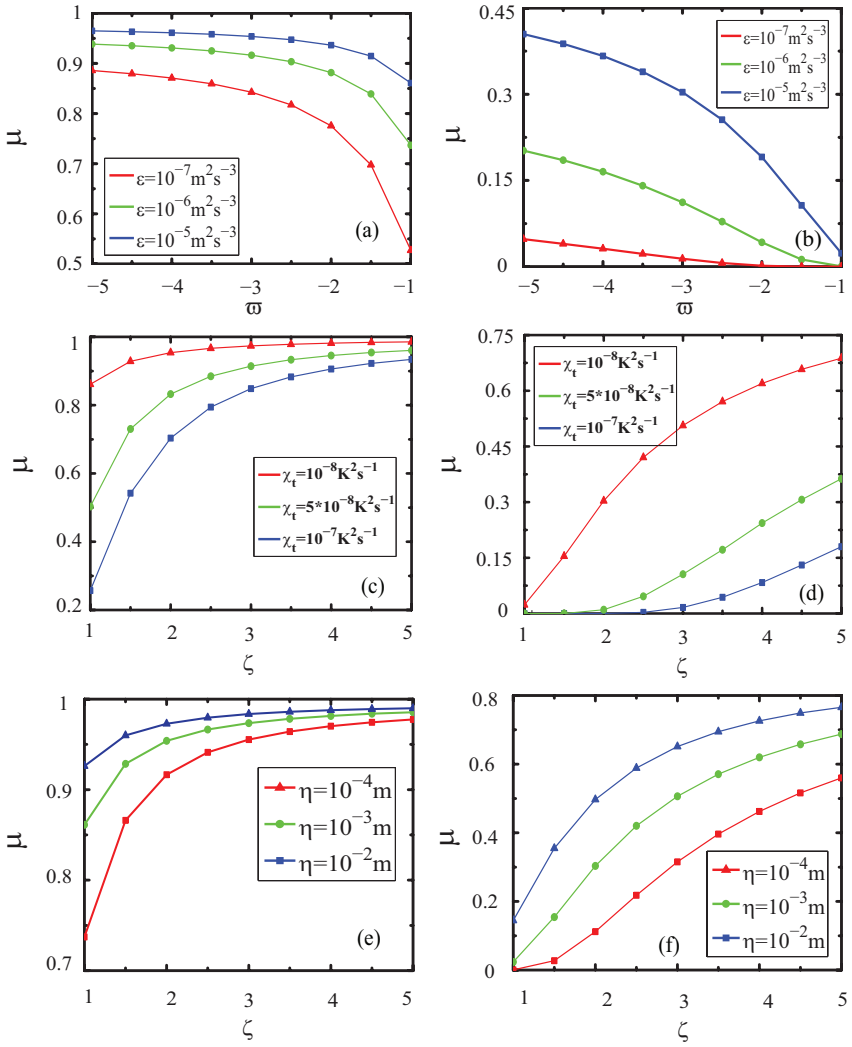

Figure 9. Spectral degree of coherence of the OAHGSM vortex beam passing through anisotropic oceanic turbulence with different ε, ϖ, χ_t, ζ, and η at z = 1200 m. Two points are fixed at $\rho_1 = (0.1\text{ cm}, 0)$, $\rho_2 = (0, 0)$ for (**a**,**c**,**e**) and $\rho_1 = (0.5\text{ cm}, 0)$, $\rho_2 = (0, 0)$ for (**b**,**d**,**f**).

4. Discussion

With the increase of the propagation distance, the OAHGSM vortex beam gradually loses its dark hollow center and evolves into a Gaussian-like beam with a larger beam spot. This is because the disturbance of turbulence and the absorption of seawater have a great influence on the beam propagation, and the general beam propagating in the turbulent channel will eventually evolve into a Gaussian-like beam [41]. The distribution of the normalized average intensity of the OAHGSM vortex beam is greatly influenced by the position factor, and the larger the position factor is, the more focused the beam is.

The results showed that the decrease of N, M, σ, and ω_0 will accelerate the evolution of the OAHGSM vortex beam into a Gaussian-like profile, which indicates that the beam with smaller N, M, σ, and ω_0 is more affected by anisotropic oceanic turbulence. Additionally, the range of the intensity distribution decreases with the increase of σ, which means that a larger σ enhances the focusing property of the OAHGSM vortex beam, similar to the results in [28].

The isotropic power spectrum of oceanic turbulence is a special case of the anisotropic one when the anisotropic coefficient $\zeta = 1$, and the results showed that the anisotropy of oceanic turbulence can improve the transmission performance of the OAHGSM vortex beam. Meanwhile, the OAHGSM vortex beam evolves into a Gaussian-like beam faster, and the spectral degree of coherence decays more rapidly under larger χ_t and ϖ and

smaller ε, ζ, and η, which is because the strength of the turbulent ocean becomes higher with the changes of the above parameters from Equation (7) and Figure 1.

The analysis results provided a theoretical basis for the parameter matching and optimization design of underwater wireless optical communication based on the OAHGSM vortex beam, so as to obtain better transmission quality.

5. Conclusions

In this paper, we derived the average intensity and the spectral degree of coherence of an OAHGSM vortex beam propagating through anisotropic oceanic turbulence based on the extended Huygens–Fresnel principle. By using numerical simulations, the effects of different beam and turbulent ocean characteristic parameters on the normalized average intensity and coherence properties of the beam were discussed in detail. Our results showed that the focusing distribution of the OAHGSM vortex beam becomes more obvious by increasing the position factor, and the beam gradually loses the initial dark hollow profile and evolves into a Gaussian-like beam due to the disturbance of oceanic turbulence with the increase of the transmission distance. Meanwhile, the cross line of the normalized average intensity of the OAHGSM vortex beam passing through anisotropic oceanic turbulence with smaller N, M, σ, and ω_0 degenerates into a Gaussian-like shape more quickly. The results also showed that smaller ε, ζ, and η and larger χ_t and ϖ correspond to higher turbulence strength, which will accelerate the beam's spreading and the decay of the spectral degree of coherence of the OAHGSM vortex beam propagating through anisotropic oceanic turbulence.

Author Contributions: X.W.: software, writing, and editing; L.W.: literature search and data analysis; S.Z.: formal analysis. All authors have read and agreed to the published version of the manuscript.

Funding: This research was funded by the National Natural Science Foundation of China (Grant No. 61871234), the Natural Science Foundation of Jiangsu Province (Grant No.BK20180755), and Open Research Fund Program of the State Key Laboratory of Low-Dimensional Quantum Physics (Grant No. KF201909).

Institutional Review Board Statement: Not applicable.

Informed Consent Statement: Not applicable.

Data Availability Statement: Not applicable.

Acknowledgments: The project funded by the Priority Academic Program Development of Jiangsu Higher Education Institutions.

Conflicts of Interest: The authors declare no conflict of interest.

References

1. Wang, H.; Peng, X.; Liu, L.; Wang, F.; Cai, Y. Twisted elliptical multi-Gaussian Schell-model beams and their propagation properties. *J. Opt. Soc. Am. A* **2020**, *37*, 89–97. [CrossRef]
2. Song, Z.; Han, Z.; Ye, J.; Liu, Z.; Liu, S.; Liu, B. Propagation properties of radially polarized multi-Gaussian Schell-model beams in oceanic turbulence. *J. Opt. Soc. Am. A* **2019**, *36*, 1719–1726. [CrossRef]
3. Hu, Z.; Liu, H.; Xia, J.; He, A.; Li, H.; Du, Z.; Chen, T.; Li, Z.; Lü, Y. Propagation characteristics of the perfect vortex beam in anisotropic oceanic turbulence. *App. Opt.* **2020**, *59*, 9956–9962. [CrossRef]
4. Ye, F.; Xie, J.; Hong, S.; Zhang, J.; Deng, D. Propagation properties of a controllable rotating elliptical Gaussian optical coherence lattice in oceanic turbulence. *Results Phys.* **2019**, *13*, 102249. [CrossRef]
5. Peng, X.; Liu, L.; Cai, Y.; Baykal, Y. Statistical properties of a radially polarized twisted Gaussian Schell-model beam in an underwater turbulent medium. *J. Opt. Soc. Am. A* **2017**, *34*, 133–139. [CrossRef] [PubMed]
6. Liu, D.; Wang, G.; Yin, H.; Zhong, H.; Wang, Y. Propagation properties of a partially coherent anomalous hollow vortex beam in underwater oceanic turbulence. *Opt. Commun.* **2019**, *437*, 346–354. [CrossRef]
7. Sun, C.; Lv, X.; Ma, B.; Zhang, J.; Deng, D.; Hong, W. Statistical properties of partially coherent radially and azimuthally polarized rotating elliptical Gaussian beams in oceanic turbulence with anisotropy. *Opt. Express* **2019**, *27*, A245–A256. [CrossRef]
8. Zhou, Y.; Zhao, D. Propagation properties of a twisted rectangular multi-Gaussian Schell-model beam in free space and oceanic turbulence. *App. Opt.* **2018**, *57*, 8978–8983. [CrossRef]

9. Tamg, M.; Zhao, D.; Li, X.; Wang, J. Propagation of radially polarized multi-cosine Gaussian Schell-model beams in non-Kolmogorov turbulence. *Opt. Commun.* **2018**, *407*, 392–397. [CrossRef]
10. Liu, Y.; Zhao, Y.; Liu, X.; Liang, C.; Liu, L.; Wang, F.; Cai, Y. Statistical characteristics of a twisted anisotropic Gaussian Schell-model beam in turbulent ocean. *Photonics* **2020**, *7*, 37. [CrossRef]
11. Huang, X.; Deng, Z.; Shi, X.; Bai, Y.; Fu, X. Average intensity and beam quality of optical coherence lattices in oceanic turbulence with anisotropy. *Opt. Express* **2018**, *26*, 4786–4797. [CrossRef] [PubMed]
12. Liu, D.; Wang, Y.; Yin, H. Evolution properties of partially coherent flattopped vortex hollow beam in oceanic turbulenc. *App. Opt.* **2015**, *54*, 10510–10516. [CrossRef] [PubMed]
13. Cheng, M.; Guo, L.; Li, J.; Huang, Q.; Cheng, Q.; Zhang, D. Propagation of an optical vortex carried by a partially coherent Laguerre-Gaussian beam in turbulent ocean. *App. Opt.* **2016**, *55*, 4642–4648. [CrossRef] [PubMed]
14. Liu, D.; Yin, H.; Wang, G.; Wang, Y. Propagation of partially coherent Lorentz-Gauss vortex beam through oceanic turbulence. *App. Opt.* **2017**, *56*, 8785–8792. [CrossRef] [PubMed]
15. Chang, H.; Yin, X.; Cui, X.; Chen, X.; Su, Y.; Ma, J.; Wang, Y.; Zhang, L.; Xin, X. Performance analysis of adaptive optics with a phase retrieval algorithm in orbital-angular-momentum-based oceanic turbulence links. *App. Opt.* **2019**, *58*, 6085–6090. [CrossRef]
16. Wang, X.; Wang, L.; Zhao, S. Research on Hypergeometric-Gaussian vortex beam propagating under oceanic turbulence by theoretical derivation and numerical simulation. *J. Mar. Sci. Eng.* **2021**, *9*, 442. [CrossRef]
17. Wang, X.; Yang, Z.; Zhao, S. Influence of oceanic turbulence on propagation of Airy vortex beam carrying orbital angular momentum. *Optik* **2019**, *176*, 49–55. [CrossRef]
18. Zhang, Y.; Guo, H.; Qiu, X.; Lu, X.; Ren, X.; Chen, L. LED-based chromatic and white-light vortices of fractional topological charges. *Opt. Commun.* **2021**, *485*, 126732. [CrossRef]
19. Zhou, H.; Fu, D.; Dong, J.; Zhang, P.; Chen, D.; Cai, X.; Li, F.; Zhang, X. Orbital angular momentum complex spectrum analyzer for vortex light based on therotational doppler effect. *Light Sci. Appl.* **2017**, *6*, e16251. [CrossRef]
20. Zhao, J.; Wang, G.; Ma, X.; Zhong, H.; Yin, H.; Wang, Y.; Liu, D. Intensity and coherence characteristics of a radial phase-locked multi-Gaussian Schell-model vortex beam array in atmospheric turbulence. *Photonics* **2021**, *8*, 5. [CrossRef]
21. Xu, Y.; Shi, H.; Zhang, Y. Effects of anisotropic oceanic turbulence on the power of the bandwidth-limited OAM mode of partially coherent modified Bessel correlated vortex beams. *J. Opt. Soc. Am. A* **2018**, *35*, 1839–1845. [CrossRef]
22. Wang, F.; Zhu, S.; Cai, Y. Experimental study of the focusing properties of a Gaussian Schell-model vortex beam. *Opt. Lett.* **2011**, *36*, 3281–3283. [CrossRef]
23. Liu, X.; Wang, F.; Liu, L.; Zhao, C.; Cai, Y. Generation and propagation of an electromagnetic Gaussian Schell-model vortex beam. *J. Opt. Soc. Am. A* **2015**, *32*, 2058–2065. [CrossRef]
24. Zhang, Y.; Liu, L.; Zhao, C.; Cai, Y. Multi-Gaussian Schell-model vortex beam. *Phys. Lett. A* **2014**, *378*, 750–754. [CrossRef]
25. Tang, M.; Zhao, D. Propagation of multi-Gaussian Schell-model vortex beams in isotropic random media. *Opt. Express* **2015**, *23*, 32766. [CrossRef] [PubMed]
26. Liu, H.; Chen, D.; Xia, J.; Lü, Y.; Zhang, L.; Pu, X. Influences of uniaxial crystal on partially coherent multi-Gaussian Schell-model vortex beams. *Opt. Eng.* **2016**, *55*, 116101. [CrossRef]
27. Huang, Y.; Zhang, B.; Gao, Z.; Zhao, G.; Duan, Z. Evolution behavior of Gaussian Schell-model vortex beams propagating through oceanic turbulence. *Opt. Express* **2014**, *22*, 17723–17734. [CrossRef] [PubMed]
28. Zheng, C. Fractional fourier transform for partially coherent off-axis Gaussian Schell-model beam. *J. Opt. Soc. Am. A* **2006**, *23*, 2161–2165. [CrossRef]
29. Cai, Y.; Lin, Q.; Baykal, Y.; Eyyuboglu, H. Off-axis Gaussian Schell-model beam and partially coherent laser array beam in a turbulent atmosphere. *Opt. Commun.* **2007**, *278*, 157–167. [CrossRef]
30. Chen, G.; Huang, X.; Xu, C.; Huang, L.; Xie, J.; Deng, D. Propagation properties of autofocusing off-axis hollow vortex Gaussian beams in free space. *Opt. Express* **2019**, *27*, 6357–6369. [CrossRef]
31. Chen, G.; Xie, J.; Cai, D.; Sun, Q.; Deng, D. Periodic propagation properties and radiation forces of focusing off-axis hollow vortex Gaussian beams in a harmonic potential. *Opt. Commun.* **2019**, *452*, 211–219. [CrossRef]
32. Li, L.; Huan, Y.; Wang, Y.; Hua, D.; Yang, X.; Liu, D.; Wang, Y. The effects of uniaxial crystal on off-axis hollow vortex Gaussian beams. *Optik* **2019**, *194*, 163133. [CrossRef]
33. Ma, X.; Wang, G.; Zhong, H.; Wang, Y.; Liu, D. The off-axis multi-Gaussian Schell-model hollow vortex beams propagation in free space and turbulent ocean. *Optik* **2021**, *228*, 166180. [CrossRef]
34. Song, Y.; Dong, K.; Chang, S.; Dong, Y.; Zhang, L. Properties of off-axis hollow Gaussian-Schell model vortex beam propagating in turbulent atmosphere. *Chin. Phys. B* **2020**, *29*, 064213. [CrossRef]
35. Lu, L.; Ji, X.; Baykal, Y. Wave structure function and spatial coherence radius of plane and spherical waves propagating through oceanic turbulence. *Opt. Express* **2014**, *22*, 27112–27122. [CrossRef] [PubMed]
36. Duntley, S. Light in the sea. *J. Opt. Soc. Am.* **1963**, *53*, 214–233. [CrossRef]
37. Li, Y.; Zhu, W.; Wu, X.; Rao, R. Equivalent refractive-index structure constant of non-Kolmogorov turbulence. *Opt. Express* **2015**, *23*, 23004–23012. [CrossRef] [PubMed]
38. Wolf, E. Unified theory of coherence and polarization of random electromagnetic beams. *Phys. Lett. A* **2003**, *312*, 263–267. [CrossRef]
39. Li, Y.; Wolf, E. Radiation from anisotropic Gaussian Schell-model sources. *Opt. Lett.* **1982**, *7*, 256–258. [CrossRef] [PubMed]

40. Andrews, L.C.; Phillips, R.L. *Laser Beam Propagation Through Random Media*; SPIE Press: Bellingham, WA, USA, 2005; Volume 152.
41. Eyyuboglu, H.T.; Baykal, Y.; Sermutlu, E. Convergence of general beams into Gaussian-intensity profiles after propagation in turbulent atmosphere. *Opt. Commun.* **2006**, *265*, 399–405. [CrossRef]